Microporous and Mesoporous Materials 200 (2014) 68–78

Contents lists available at ScienceDirect

Microporous and Mesoporous Materials

journal homepage: www.elsevier.com/locate/micromeso

Introducing a self-consistent test and the corresponding modification in the Barrett, Joyner and Halenda method for pore-size determination

Jhonny Villarroel-Rocha, Deicy Barrera, Karim Sapag *

Laboratorio de Sólidos Porosos, Instituto de Física Aplicada, CONICET, Universidad Nacional de San Luis, Chacabuco 917, 5700 San Luis, Argentina

ARTICLE INFO

Article history:
Received 22 April 2014
Received in revised form 6 August 2014
Accepted 7 August 2014
Available online 15 August 2014

Keywords:
Ordered mesoporous materials
Mesopores size distribution
Nitrogen adsorption–desorption isotherms
Kelvin equation

ABSTRACT

A standard method to obtain the mesopore size distribution of adsorbents is the Barrett, Joyner and Halenda (BJH) analysis of the N_2 adsorption–desorption isotherm at 77 K. The availability, over the last two decades, of well-defined model adsorbents in the mesopore range, together with other forms of isotherm analysis with the help of the Density Functional Theory (DFT) has shown that the BJH method tended to underestimate the pore-width when they are smaller than 10 nm. Regarding this fact, we have reported an improved BJH method, where we have remarked that the reconstruction of the adsorption–desorption isotherm from the BJH results leads to some inconsistency. We therefore proposed a simple means to cancel the mentioned discrepancy and inconsistency. This correction can be made by simply adding a corrective term to the standard BJH equation, which value is selected to meet a self-consistent criterion, i.e. the reconstructed isotherm should fit the original one. In the first article, the method was applied for some ordered mesoporous materials (OMM) synthesized in our laboratory, showing only the results without major details. In this work, we validate the test for other samples, in other pore size ranges, introducing some remarks in theoretical aspects and in the importance of obtaining and taking into account the micropore volume. Finally, a detailed procedure to apply the proposal method using only the experimental data of the analysis is presented.

1. Introduction

Among the most important textural characteristics of porous materials is their Pore Size Distribution (PSD), which defines the pore volumes for each pore size. The most used methods to obtain the PSD of nanoporous materials are based on the N_2 adsorption–desorption experimental isotherm data at 77 K, where important researches have been carried out in order to apply different theories. The used methods to evaluate the PSD can be divided into two groups, those that uses molecular theories (microscopic methods) [1,2] and those based on the theory of the capillary condensation (macroscopic methods) [3,4].

The most used microscopic method is based on the Non-Local Density Functional Theory (NLDFT) [5–7], which describes the configuration of the adsorbed phase at molecular level. By using the NLDFT method a reliable PSD can be obtained if the kernel (simulated isotherms of different pore sizes with specific geometry corresponding to a determined interaction adsorbate–adsorbent) is adequately chosen [8]. However, if the set of isotherms (kernel) are not available or if the commercial gas adsorption instruments are not equipped with the corresponding software it is not easy to apply this microscopic method.

Among the macroscopic methods, the first one proposed to determine the PSD in mesoporous materials was introduced by Barrett, Joyner and Halenda (BJH), based on the capillary condensation theory, using the Kelvin equation, where a cylindrical pore geometry is assumed and the desorption branch data of the isotherm are used [9]. The equation used in the BJH method was modified by Montarnal [10] taking into accounts not only the pore radio but also the length of the pores. Dollimore and Heal using the Montarnal's equation in the BJH method introduced the Dollimore-Heal method (DH) [11]. However, it was found that these macroscopic methods overestimate the capillary condensation/evaporation pressure and subsequently the pore size is underestimated (up to 25% for mesoporous materials consisting of pores $\leqslant$10 nm) [1,2,12,13].

Among the nanoporous materials are the ordered mesoporous materials (OMM), which have attracted attention in materials science due to their interesting textural, structural and morphological properties. These special characteristics are related to highly ordered pore structures, tunable pore size, high specific surface

* Corresponding author. Tel.: +54 2664 520300x6125; fax: +54 2664 436151.
E-mail address: sapag@unsl.edu.ar (K. Sapag).

http://dx.doi.org/10.1016/j.micromeso.2014.08.017
1387-1811/

areas, large pore volumes and narrow pore size distribution. OMM have found wide potential applications in adsorption, catalysis supports, molecular separation, nano-reactors and particularly in reactions involving large and bulky molecules [14–16]. Regarding to their applications, one of the most important properties to be analyzed is their PSD [17–19], which states the size of the molecules that can act inside the chosen material.

Kruk, Jaroniec and Sayari working with OMM MCM-41 type, proposed to add a fixed value to the pore radius obtained by the BJH method using the adsorption branch data of OMM silica-based [13]. This fixed value was determined by a calibration procedure using the pore size data, obtained by X-ray diffraction (XRD) and nitrogen adsorption data, and the filling relative pressure for primary mesopores in an OMM series of MCM-41 type. But, we have found that this proposed fixed value is not the same for all the OMM, being necessary to estimate it for each kind of material.

In order to avoid the use of additional characterization techniques to the nitrogen adsorption–desorption experiments, a new method (Villarroel-Barrera-Sapag -VBS method-) to the PSD analysis for mesoporous materials has been introduced [20]. This is an improved method in comparison with traditional methods such as BJH and DH. In these traditional methods, the pore radius (r_P) is calculated by the sum of the Kelvin radius (r_K) and the statistical film thickness of adsorbed nitrogen (t). Taking into account that the t value is obtained from experimental data, the underestimation is given by the r_K itself (obtained by unmodified/original Kelvin equation). In order to avoid this underestimation, the VBS method adds a correction term, f_c, to the original Kelvin equation. Furthermore, unlike the BJH method the VBS method considers appropriate mechanisms of capillary condensation and evaporation in the mesopores (for cylindrical and spherical pores) and introduces an additional equation for materials with spherical pore geometry. In addition, this method also takes into account the presence of micropores in some of the OMM. For different mesoporous materials synthesized in our laboratory, the PSD obtained by applying the VBS method agreed with those obtained by NLDFT method [20,21]. However, the selected samples tested in that first article were not very ordered and they had a restricted range of pore size (up to 8 nm for cylindrical pores and up to 4 nm for spherical pores). As the DFT method for spherical pores was developed for pore sizes higher than 5 nm, the comparison between VBS and DFT is not definitive to conclude the effectiveness of the former method. In all cases, the advantage of the VBS method (macroscopic method) compared to the NLDFT method (microscopic method) is that it does not require a predetermined kernel to be applied. Furthermore, in that first article, the VBS method was introduced and applied for some synthesized samples without giving major details and, consequently, several authors wrote to us asking for further information.

In the present work, the VBS method procedure is completely explained in detail and further information is given, in order to facilitate its application to obtain suitable PSD for silica-based ordered mesoporous materials with both, cylindrical or spherical pore geometry using N_2 adsorption–desorption experimental isotherm data. The importance of taking into account an adequate calculus of the micropore volume for mesoporous materials with this class of pores is highlighted and explained. Furthermore, the method was tested for five well known OMM samples published by other authors, extending the range of the pore size analysis. In this case the selected samples with spherical pores had pore sizes of 9.5 and 15 nm then the comparison with DFT method is adequate. The PSDs obtained using the VBS method were compared with those obtained by NLDFT, remarking the effectiveness of the VBS method, which use only the experimental isotherm data.

2. Materials and methods

2.1. Materials

In order to exemplify the VBS method, data of OMM samples previously reported were chosen. The selected OMM isotherms data with cylindrical pore geometry were SBA-15_S3 [21], MCM-41B [22] and SE3030 [23]; and with spherical pore geometry were SBA-16 [24] and KLE [23].

2.2. Experimental isotherms

Experimental isotherms of OMM with cylindrical and spherical pore geometries are shown in Figs. 1 and 2. All the studied samples exhibits Type IV isotherms, which are typical of mesoporous materials and present hysteresis loops (except the MCM-41B). The SBA-15_S3 sample exhibits a Type H1 hysteresis loop, often associated to a defined primary mesopore size; the SE3030, SBA-16 and KLE samples show a Type H2 hysteresis loop. In these samples there is a presence of cavitation phenomena on the desorption branch [23].

2.3. Calculations of textural properties

Textural properties of the OMM under study were determined from nitrogen adsorption–desorption isotherms data at 77 K. The

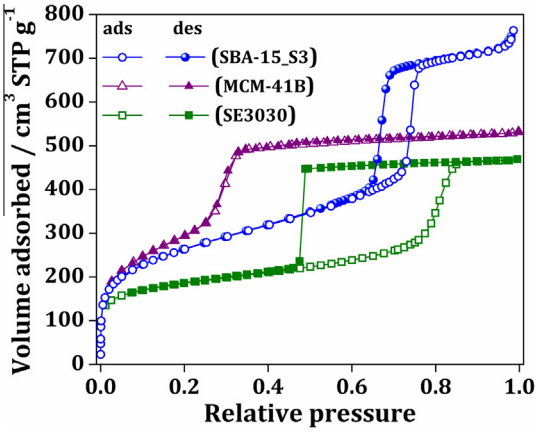

Fig. 1. Nitrogen adsorption–desorption experimental isotherms at 77 K of OMM with cylindrical pores.

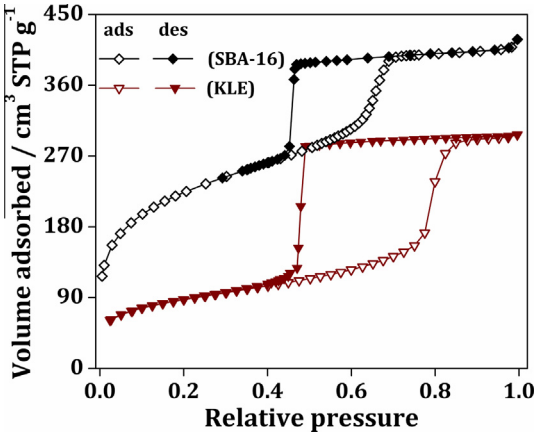

Fig. 2. Nitrogen adsorption–desorption experimental isotherms at 77 K of OMM with spherical pores.

specific surface area (S_{BET}) was estimated by the Brunauer, Emmet and Teller (BET) method [25] using the relative pressure ranges from 0.05 to 0.17 (SBA-15_S3), 0.05 to 0.20 (MCM-41B), 0.05 to 0.13 (SE3030) and 0.05 to 0.15 (SBA-16 and KLE), obtained using the considerations proposed by Rouquerol et al. [26]. The total pore volume (V_T) was obtained by Gurvich's rule [4] at a relative pressure of 0.98. The micropore volume ($V_{\mu p}$) was calculated by means of the α_s-plot method [3] using the LiChrospher Si-1000 macroporous silica gel as the reference adsorbent [27]. The α_s-plot method was applied from the first α_s value above of the *point B* (calculated by Eq. 6.4 of [4]), because at this point the micropores have been fully filled, until the best linear fit is obtained [28]. These criteria are shown in the α_s-plot for the SBA-15_S3 sample (Fig. 3), where the primary mesopores volume (V_{pmp}) is also shown. The ranges of α_s values for each sample under study were from 0.68 to 0.80 (SBA-15_S3), 0.58 to 0.90 (SE3030), 0.63 to 0.74 (KLE) and 0.68 to 0.95 (SBA-16).

The PSD of the OMM obtained by VBS method, were compared with the ones obtained by NLDFT method. This last method is included in ASiQwin software, v. 2.0 (Quantachrome Instruments). The kernels used for cylindrical pore geometry were: *N_2 at 77 K on silica, cylindrical pore, NLDFT adsorption* [29] and *desorption branch* [30]. For spherical pore geometry the kernel used was *N_2 at 77 K on silica, cylindrical/spherical pore, NLDFT adsorption branch* [24].

The selection of the suitable branch in the PSD studies has been subject of several discussions by other authors, justifying the use of adsorption or desorption branches [13,30]. When both branches can be selected, the selection of the desorption branch is the most accepted because it reflects transitions near the equilibrium phase.

When the hysteresis loop for nitrogen isotherms at 77 K closing near to 0.40–0.45, in relative pressure, the usage of the desorption branch should be carefully analyzed to ensure that this fact is due to the pore size. For example, the cavitation phenomenon can be present and the PSD of desorption branch produces an artifact. In these cases, the better chosen branch is the adsorption one.

The PSD evaluation for MCM-41B and SBA-15_S3 samples can be performed using adsorption and desorption branches, but the SE3030, SBA-16 and KLE samples were only analyzed using the adsorption branch, because the cavitation phenomenon is present in the desorption branch [23,24].

The branch data to select in the PSD analysis are those that provide information about the pore sizes, regardless of the adsorptive and the analysis conditions. Then, to select the "correct" branch data is necessary to analyze each case.

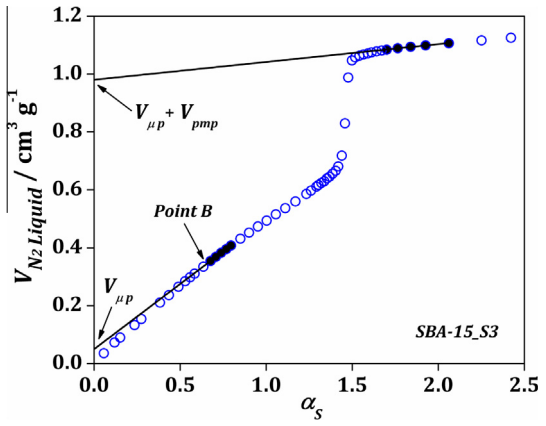

Fig. 3. α_s-plot of the SBA-15_S3 sample. Filled symbols **(•)** represent the selected range of α_s values.

3. VBS method – description

The VBS method for the PSD evaluation is proposed to be used in OMM silica-based samples with cylindrical and spherical pore geometries. This method, based on the BJH algorithm, considers appropriate mechanisms of capillary condensation and evaporation (for cylindrical and spherical pores) in the mesopores, by means of the corresponding Kelvin equation. The VBS method modifies this equation with the addition of a correction term (f_c) to obtain the pore radius.

A *data base* with information of the pore volume for each pore size is obtained from the modified Kelvin equation (r_K) with a selected f_c value, the statistical film thickness of adsorbed nitrogen (t), the completed nitrogen isotherm data (of the chosen branch) and an appropriate expression to estimate the pore volume (ΔV_p). From this data base, a *simulated isotherm* (corresponding to the selected f_c value) of the proper adsorption or desorption branch is constructed. Then, a series of simulated isotherms with different values of f_c are obtained by this method. Using this set of isotherms it is possible to find the *final correction term* that adjusts to the experimental one (validating the self-consistency of the method). Finally, with the experimental isotherm data and the final correction term value, the *pore size distribution* (dV_p/dw_p vs. $\overline{w}_p$) is obtained, where dV_p/dw_p is the change of the pore volume related to the pore size and, $\overline{w}_p$ is the mean pore size, following the BJH mechanism. The whole detailed procedure of the VBS method is explained in the Appendix.

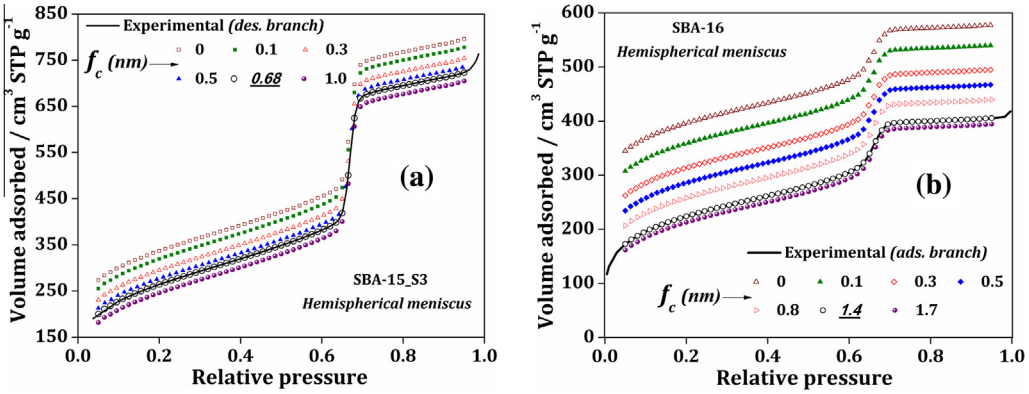

Fig. 4. Set of simulated isotherms using different correction terms (f_c in nm). Experimental and simulated isotherms for: (a) desorption branch of the SBA-15_S3 sample and (b) adsorption branch of the SBA-16 sample.

Table 1
Textural properties of OMM under study.

Material	S_{BET} ($m^2\ g^{-1}$)	$V_{\mu p}$ ($cm^3\ g^{-1}$)	V_{pmp} ($cm^3\ g^{-1}$)	V_T ($cm^3\ g^{-1}$)
SBA-15_S3	955	0.05	0.93	1.15
MCM-41B	1070	0	0.69	0.82
SE3030	675	0.13	0.57	0.72
SBA-16	815	0.09	0.48	0.63
KLE	320	0.02	0.40	0.46

Table 2
Final correction terms of OMM under study.

Material	f_c (nm)	
	Ads	Des
SBA-15_S3	1.19	0.67
MCM-41B	0.88	0.54
SE3030	1.54	–
SBA-16	1.40	–
KLE	2.19	–

4. Results and discussion

The results obtained by the application of the VBS method using the Tables A.1–A.3 for the selected samples are presented.

Fig. 4(a) and (b) shows a set of simulated isotherms obtained by the VBS method. These examples are given for materials with cylindrical (SBA-15_S3) and spherical pore geometries (SBA-16), taking into account all the criteria previously discussed. Adsorption and desorption branches were used for SBA-16 and SBA-15_S3 samples, respectively. These isotherms were simulated using different correction terms values (f_c) between 0 and 1.0 nm for SBA-15_S3 sample (Fig. 4(a)) and between 0 and 1.7 nm for SBA-16 sample (Fig. 4(b)). As it may be seen, when the unmodified Kelvin equation is used ($f_c = 0$), the adsorbed volume is overestimated and subsequently the pore size is underestimated. This overestimation decreases as the correction term increases and the final correction term f_c is obtained when the simulated isotherm agrees with the experimental one.

The final f_c values found for each material are shown in Table 2. It can be seen that these f_c values differ from one sample to another and that they are different for each branch of the isotherm as well. It is noticeable that, for materials where both branches were studied, the f_c values are higher in the adsorption branch than in the desorption one.

For all the materials under study, the PSD were obtained by VBS and NLDFT methods. This comparison was carried out because the last microscopic method mentioned is one of the most suitable for the PSD analysis of this kind of materials [5–7].

The PSD for *cylindrical pore geometry*, SBA-15_S3, MCM-41B and SE3030, are shown in Fig. 5(a)–(c), respectively. In these figures it can be seen a good agreement between the results obtained by using the VBS method and the NLDFT method. Regarding to the MCM-41B (Fig. 5(b)), which is the sample with the smallest pore size; higher differences are observed between both methods. An important fact to highlight is that in these cases the adsorption and desorption mechanisms are the same.

The PSD for OMM with *spherical pore geometry*, SBA-16 and KLE are shown in Fig. 6(a) and (b), respectively. As well as in materials with cylindrical pores, the VBS method also gives suitable results for the PSD evaluation, taking into account that they agree with the reliable NLDFT method. The sample with a higher modal pore size (KLE sample) exhibited a minor agree between both methods.

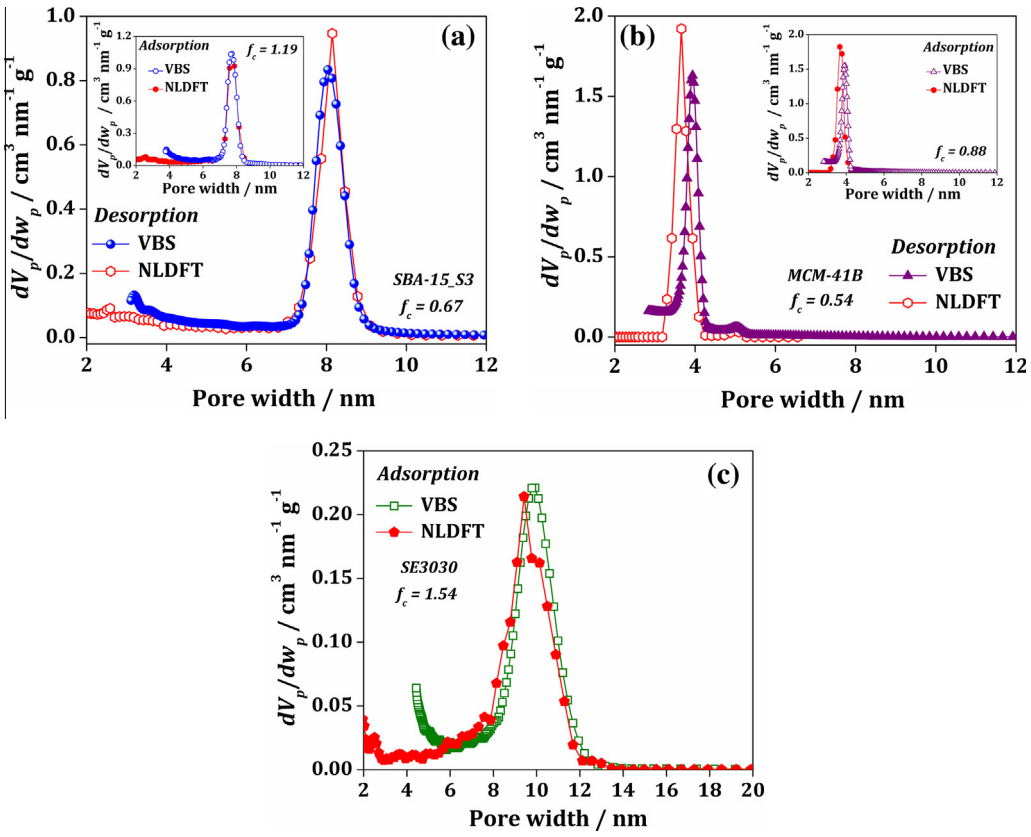

Fig. 5. Comparison of the PSD obtained by VBS and NLDFT methods for chosen branches of: (a) SBA-15_S3 sample ($f_{c\text{-ads}} = 1.19$; $f_{c\text{-des}} = 0.67$), (b) MCM-41B sample ($f_{c\text{-ads}} = 0.88$; $f_{c\text{-des}} = 0.54$) and (c) SE3030 sample ($f_{c\text{-ads}} = 1.54$).

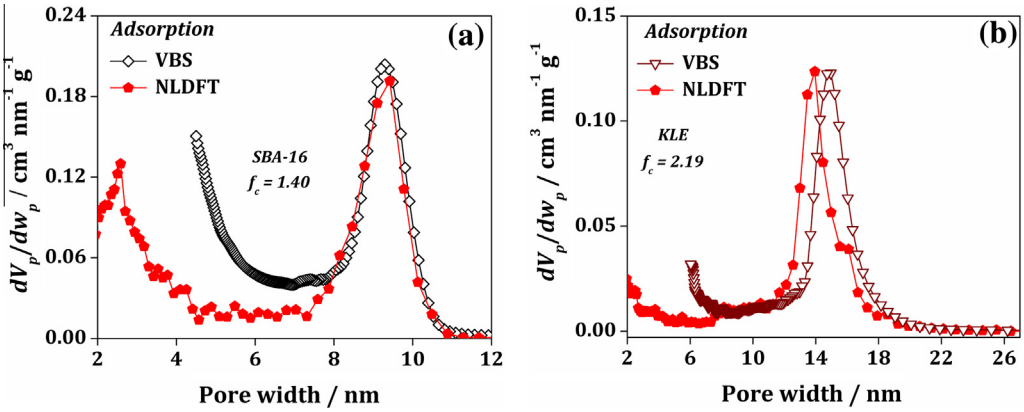

Fig. 6. Comparison of the PSD obtained by VBS and NLDFT methods for adsorption branch of: (a) SBA-16 sample (f_c = 1.40) and (b) KLE sample (f_c = 2.19).

Table 3
Primary mesopore sizes (w_p) obtained by VBS, NLDFT and BJH methods.

Material	VBS (nm)		NLDFT (nm)		BJH (nm)
	Ads	Des	Ads	Des	
SBA-15_S3	7.7	8.0	7.7	8.1	6.6
MCM-41B	3.8	3.9	3.7	3.7	2.8
SE3030	9.8	–	9.4	–	11.2*
SBA-16	9.3	–	9.4	–	6.4*
KLE	14.7	–	13.9	–	10.3*

* From adsorption branch data.

Table 3 summarizes the primary mesoporous sizes obtained by VBS, and traditional microscopic and macroscopic methods as NLDFT and BJH respectively. Results obtained by BJH method underestimated the primary mesopores size of all the samples under study with both cylindrical and spherical pore geometries, except for the SE3030 sample. The underestimation of BJH is between 18% and 22% for cylindrical and between 26% and 32% for spherical pore geometries, respect to NLDFT method. This underestimation has been previously reported [31]. The difference of the modal pore size obtained by VBS and NLDFT methods is about 1–5% .

5. Conclusions

The VBS method to obtain a suitable PSD for ordered mesoporous materials with cylindrical or spherical pore geometries has been tested and the results agree with the PSD evaluated by NLDFT method.

The complete procedure to apply the VBS method for the PSD evaluation of OMM was explained in detail, using specific samples to exemplify it.

The importance of the application of this method includes the correct selection of the capillary condensation or evaporation mechanisms corresponding to the chosen isotherm branch and the considered pore geometry.

It is remarkable that, the VBS method in contrast to the traditional macroscopic methods can accurately reproduce the experimental isotherm (validating its self-consistency) from the PSD data obtained by this method (as shown in Fig. 4).

Among the advantages of the use of this method is the versatility showed for OMM with different pore geometries. Moreover, the VBS method could be applied using different gases and temperatures.

In this method, a correction term (f_c) was added and adjusted to obtain self-consistency with experimental data. Further studies could be focused on finding the physical meaning of the final correction term or an equivalent quantity that can adjust the PSD with experimental data, compensating the underestimation of the pore size. Perhaps, this value can be associated with the porous structure of the material, for instance with the connectivity between the pores, which has not been considered in this study.

Acknowledgement

Authors are grateful to Dr. Matthias Thommes (Quantachrome Instruments), who kindly provided the experimental isotherms data.

This work was financially supported by Universidad Nacional de San Luis (UNSL), Agencia Nacional de Promoción Científica y Tecnológica (ANPCyT) and Consejo Nacional de Investigaciones Científicas y Técnicas (CONICET) from Argentina.

Appendix A. VBS method – procedure

The entire methodology to obtain the PSD for materials with cylindrical and spherical pore geometries by using the VBS method is described as follows.

A.1. Data base

By using BJH method the relative pressure of filling or emptying pore sizes around 2 nm (lower limit of mesopores) is approximately 0.1. Taking into account that this method overestimates the capillary condensation/evaporation pressure (underestimating the pore size), a minimal relative pressure value of ***0.05*** was chosen.

The experimental data of relative pressure (p/p^0) and amount adsorbed (V_{STP}) are collected from the chosen branch (adsorption or desorption) of the N_2 adsorption–desorption isotherm at 77 K. In order to have more points in the experimental isotherm, some points were added in the range from 0.050 to 0.955 by a non-linear interpolation at intervals of 0.005 of p/p^0 (for instance, by non-linear interpolation add-in in Excel Microsoft® software). The obtained isotherms are named completed isotherms.

A.1.1. Cylindrical pores

PSD evaluation of OMM with cylindrical pores can be performed using either the adsorption or desorption branch. In the adsorption branch the capillary condensation is ruled by the formation of *cylindrical* meniscus while, in the desorption branch, the evaporation phenomena is ruled by the formation of *hemispherical* meniscus [3,32]. Therefore, following the proposed VBS method, the Kelvin radius (r_K) for a cylindrical (adsorption branch) or

hemispherical (desorption branch) meniscus, is modified by the addition of a correction term (f_c) as is shown in Eqs. (A.1) and (A.2), respectively.

$$r_K = -\frac{\gamma \cdot V_L}{R \cdot T \cdot \ln\left(\frac{p}{p^0}\right)} + f_c = -\frac{0.48103}{\ln\left(\frac{p}{p^0}\right)} + f_c \quad (A.1)$$

$$r_K = -\frac{2 \cdot \gamma \cdot V_L}{R \cdot T \cdot \ln\left(\frac{p}{p^0}\right)} + f_c = -\frac{0.96207}{\ln\left(\frac{p}{p^0}\right)} + f_c \quad (A.2)$$

where r_K is expressed in nm, γ and V_L are the surface tension, $8.88{\cdot}10^{-3}$ J m^{-2}, and the molar volume of the liquid nitrogen, $3.468{\cdot}10^{22}$ nm^3 mol^{-1}, respectively; R is the ideal gas constant, $8.3143{\cdot}10^{18}$ J nm^2 (K mol m^2)$^{-1}$ and T is the absolute temperature of adsorption, 77 K [33]. Then, the pore radius (r_p), expressed in nm, was calculated by the sum of the corresponding modified Kelvin radius and the statistical film thickness of adsorbed nitrogen (t), as is shown in Eq. (A.3).

$$r_p = r_K + t \quad (A.3)$$

where t value (for nitrogen at 77 K on OMM silica-based), expressed in nm, was estimated by Eq. (A.4), using the Harkins–Jura equation adjusted by Kruk et al. [13].

$$t = 0.1 \cdot \left[\frac{60.65}{0.03071 - \log\left(\frac{p}{p^0}\right)}\right]^{0.3968} \quad (A.4)$$

(Fig. A.1) shows a comparison between statistical film thickness of nitrogen adsorbed calculated from Eq. (A.4) and that obtained by LiChrospher Si-1000 macroporous silica data [27]. In this figure it is shown that the Eq. (A.4) provides very good results for this kind of materials in most of the relative pressure range in which the VBS method is applied, except in the extremes of low and high pressures.

From Eqs. (A.1)–(A.4) the BJH algorithm was applied to obtain the change in the filling or emptying volumes (ΔV_p) of cylindrical pores using the Eq. (A.5), which assumed the Montarnal's modification [16].

$$\Delta V_{p_n} = \left(\Delta V_n - \Delta t_n \cdot \sum_{i=1}^{n-1} \frac{2 \cdot \Delta V_{p_i}}{\bar{r}_{p_i}} + \Delta t_n \cdot \bar{t}_n \cdot \sum_{i=1}^{n-1} \frac{2 \cdot \Delta V_{p_i}}{\left(\bar{r}_{p_i}\right)^2}\right) \cdot \left(\frac{\bar{r}_{p_n}}{\bar{r}_{p_n} - t_n}\right)^2 = [\Delta V_n - (D - E)] \cdot Q \quad (A.5)$$

where at the *n-th* stage, ΔV_n corresponds to the change of the adsorbed nitrogen volume (as liquid); Δt_n is the change in the thickness of the adsorbed layer on the pore walls; $\bar{r}_{p_n}$ is the average pore radius; and $\bar{t}_n$ is the average thickness of the adsorbed layer. The value of ΔV_{p_n} corresponds to the pore volume for the $\bar{r}_{p_n}$ pore radius. The expressions for Q, D and E, are shown in Eqs. (A.6)–(A.8), respectively.

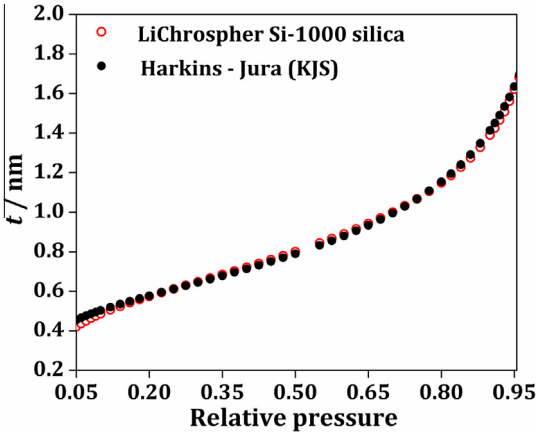

Fig. A.1. Comparison of statistical film thickness of nitrogen adsorbed calculated from Harkins–Jura equation and LiChrospher Si-1000 macroporous silica data.

$$Q = \left(\frac{\bar{r}_{p_n}}{\bar{r}_{p_n} - t_n}\right)^2 \quad (A.6)$$

$$D = \Delta t_n \cdot \sum_{i=1}^{n-1} \frac{2 \cdot \Delta V_{p_i}}{\bar{r}_{p_i}} = \Delta t_n \cdot \sum_{i=1}^{n-1} \Delta A_{p_i} \quad (A.7)$$

$$E = \Delta t_n \cdot \bar{t}_n \cdot \sum_{i=1}^{n-1} \frac{2 \cdot \Delta V_{p_i}}{\left(\bar{r}_{p_i}\right)^2} = \Delta t_n \cdot \bar{t}_n \cdot \sum_{i=1}^{n-1} \frac{\Delta A_{p_i}}{\bar{r}_{p_i}} \quad (A.8)$$

where ΔA_{p_n} corresponds to the pore area (based on the geometry of the cylinder) for the pore radius ($\bar{r}_{p_n}$) determined by the Eq. (A.9).

$$\Delta A_{p_n} = \frac{2 \cdot \Delta V_{p_n}}{\bar{r}_{p_n}} \quad (A.9)$$

Describing the Eq. (A.5), the term $(D - E)$ refers to the change of multilayer adsorbed volume of cylindrical pores larger than $\bar{r}_{p_n}$, thus the term $\Delta V_n - (D - E)$ is the change in the volume by capillary condensation or evaporation inside the $\bar{r}_{p_n}$. Therefore, this last term is corrected by multiplying by Q, in order to consider the multilayer adsorption in $\bar{r}_{p_n}$ obtaining its pore volume ΔV_{p_n}.

Finally, the equivalent length (L_{p_n}) of the cylindrical pore radius ($\bar{r}_{p_n}$) was calculated with the Eq. (A.10).

$$L_{p_n} = \frac{\Delta V_{p_n}}{\pi \cdot \left(\bar{r}_{pn}\right)^2} = \left(\frac{1}{2 \cdot \pi}\right) \cdot \left(\frac{\Delta A_{p_n}}{\bar{r}_{pn}}\right) \quad (A.10)$$

Once the whole range of p/p^0 is covered, the *data base* ($\bar{r}_{p_n}$, L_{p_n}) is obtained. In order to exemplify this methodology, in the Table A.1 the detailed mathematical steps to obtain this data base for SBA-15_S3 sample is shown. In this case, the completed desorption branch data of the experimental nitrogen isotherm was chosen selecting a f_c value of 0.3 nm.

In Table A.1, columns {1} and {10} are the completed nitrogen isotherm data (range between 0.050 and 0.955 of p/p^0 at intervals of 0.005). Column {2} is one of the most important to take into account in the VBS method; the modified Kelvin equation should be chosen according to the mechanisms of filling/emptying above mentioned. Columns {2} to {19} are calculated for the application of Eq. (A.5) by means of the BJH algorithm. Obtaining the last mentioned values, the data base for cylindrical pores ($\bar{r}_{p_n}$, L_{p_n}) can be obtained, which values are given in columns {5} and {20}, respectively.

A.1.2. Spherical pores

PSD evaluation of OMM with spherical pores by using the VBS method was only applied for the adsorption branch, (because of the presence of cavitation phenomenon on desorption branch) where the capillary condensation is ruled by the formation of hemispherical menisci [34,35].

From adsorption branch data, the pore radius (r_p), expressed in nm, was calculated using the Eqs. (A.2)–(A.4). Then, from these equations, the BJH algorithm was applied using the expression of the change in the filling volume (ΔV_p) for spherical pores (Eq. (A.11)), previously published by the authors [20].

$$\Delta V_p = [\Delta V_n - (F - G + H)] \cdot R \quad (A.11)$$

where the expressions for R, F, G and H, are shown in Eqs. (A.12)–(A.15), respectively.

Table A.1
Calculation of the data base ($\bar{r}_{p_n}$, L_{p_n}) for OMM with *cylindrical pores*, using a correction term value (f_c) of 0.3 nm.

	{1}	{2}	{3}	{4}	{5}	{6}	{7}	{8}	{9}	{10}	{11}	{12}	{13}	{14}	{15}	{16}	{17}	{18}	{19}	{20}	{21}
	p/p^0	r_K	r_p	Δr_p	$\bar{r}_p$	t	Δt	$\bar{t}$	Q	V	ΔV	D	E	ΔV_p	$\Sigma\Delta V_p$	ΔA_p	$\Sigma\Delta A_p$	$\Delta A_p/\bar{r}_p$	$\Sigma(\Delta A_p/\bar{r}_p)$	L_p	dV_p/dw_p
		(nm)								($mm^3\ g^{-1}$)						($m^2\ g^{-1}$)		($m^2\ g^{-1}\ nm^{-1}$)			($mm^3\ g^{-1}\ nm^{-1}$)
0	0.955	21.19	22.86			1.66				1121.6					0		0		0		
1	0.950	19.06	20.69	2.17	21.78	1.64	0.029	1.65	1.17	1118.6	2.9	0	0	3.42	3.42	0.31	0.31	0.014	0.014	0.0023	3.2
2	0.945	17.31	18.91	1.78	19.80	1.61	0.027	1.62	1.18	1116.2	2.5	0.009	0.0006	2.92	6.34	0.30	0.61	0.015	0.029	0.0024	3.3
3	0.940	15.85	17.43	1.48	18.17	1.58	0.026	1.60	1.20	1114.0	2.2	0.016	0.0012	2.62	8.96	0.29	0.90	0.016	0.045	0.0025	3.5
4	0.935	14.61	16.17	1.26	16.80	1.56	0.025	1.57	1.21	1112.0	2.0	0.022	0.0017	2.36	11.3	0.28	1.18	0.017	0.062	0.0027	3.8
.	...	...	...	...	...	...	...	...	...	...	...	...	...	...	...	...	...	...	...	...	...
.	0.680	2.79	3.76	0.055	3.79	0.969	0.006	0.972	1.80	964.5	37.0	0.445	0.095	66.1	248.4	34.9	106.3	9.2	24.9	1.47	$2.43{\cdot}10^3$
.	0.675	2.75	3.71	0.053	3.74	0.963	0.006	0.966	1.81	905.1	59.3	0.653	0.148	106.8	355.1	57.1	163.4	15.3	40.2	2.43	$4.03{\cdot}10^3$
.	0.670	2.70	3.66	0.052	3.68	0.957	0.006	0.960	1.82	836.6	68.5	0.990	0.234	123.6	478.7	67.1	230.5	18.2	58.4	2.90	$4.80{\cdot}10^3$
.	0.665	2.66	3.61	0.050	3.63	0.951	0.006	0.954	1.83	771.0	65.6	1.376	0.333	118.4	597.2	65.2	295.7	17.9	76.4	2.85	$4.73{\cdot}10^3$
.	0.660	2.62	3.56	0.049	3.58	0.945	0.006	0.948	1.84	715.7	55.3	1.740	0.426	99.6	696.7	55.5	351.2	15.5	91.9	2.47	$4.09{\cdot}10^3$
.	0.655	2.57	3.51	0.047	3.54	0.939	0.006	0.942	1.85	675.3	40.4	2.037	0.502	72.0	768.7	40.7	391.9	11.5	103	1.83	$3.04{\cdot}10^3$
.	...	...	...	...	...	...	...	...	...	...	...	...	...	...	...	...	...	...	...	...	...
.	0.065	0.652	1.123	0.015	1.131	0.471	0.005	0.474	2.94	325.2	4.4	3.576	0.674	4.30	1102.4	7.60	717.4	6.7	289	1.07	579
$n-2$	0.060	0.642	1.108	0.015	1.116	0.466	0.005	0.469	2.95	320.6	4.6	3.756	0.709	4.66	1107.1	8.35	725.7	7.5	296	1.19	611
$n-1$	0.055	0.632	1.092	0.016	1.100	0.461	0.005	0.464	2.96	315.6	5.0	3.967	0.751	5.22	1112.3	9.50	735.2	8.6	305	1.37	664
n	0.050	0.621	1.076	0.016	1.084	0.455	0.006	0.458	2.97	310.2	5.4	4.218	0.801	5.88	1118.2	10.9	746.0	10.0	315	1.59	722

Column {1}: p/p^0 values from 0.955 to 0.050 (with intervals of 0.005).
Column {2}: Calculated from modified Kelvin equation corresponding to chosen branch, adsorption or desorption, with the Eqs. (A.1) or (A.2), respectively), using the selected f_c value. In this example, the Eq. (A.2) is applied (because desorption branch data are used) using a $f_c = 0.3$ nm.
Column {3}: From Eq. (A.3). $r_p = r_K + t = \{2\} + \{6\}$.
Column {4}: $\Delta r_p = r_{p(n-1)} - r_{p(n)} = \{3\}_{(n-1)} - \{3\}_{(n)}$, ($\{3\}_{(n-1)}$ from row above).
Column {5}: $\bar{r}_p = 0.5{\cdot}(r_{p(n-1)} + r_{p(n)}) = 0.5{\cdot}(\{3\}_{(n-1)} + \{3\}_{(n)})$, ($\{3\}_{(n-1)}$ from row above).
Column {6}: Calculated from Eq. (A.4).
Column {7}: $\Delta t = t_{(n-1)} - t_{(n)} = \{6\}_{(n-1)} - \{6\}_{(n)}$, ($\{6\}_{(n-1)}$ from row above).
Column {8}: $\bar{t} = 0.5{\cdot}(t_{(n-1)} + t_{(n)}) = 0.5{\cdot}(\{6\}_{(n-1)} + \{6\}_{(n)})$, ($\{6\}_{(n-1)}$ from row above).
Column {9}: From Eq. (A.6). $Q = [\bar{r}_p/(\bar{r}_p - t)]^2 = [\{5\}/(\{5\} - \{6\})]^2$.
Column {10}: Amount adsorbed (as liquid) from the chosen branch of the isotherm (adsorption or desorption). $V\ (mm^3\ g^{-1}) = V_{STP}\ (cm^3\ g^{-1}){\cdot}1.5468$. STP: Standard Temperature and Pressure. In this example the taken values (interpolated from experimental isotherm data) are of the SBA-15_S3 sample (desorption branch).
Column {11}: $\Delta V = V_{(n-1)} - V_{(n)} = \{10\}_{(n-1)} - \{10\}_{(n)}$, ($\{10\}_{(n-1)}$ from row above).
Column {12}: From Eq. (A.7). $D = 0.01{\cdot}\Delta t_{(n)}{\cdot}(\Sigma\Delta A_p)_{(n-1)} = 0.01{\cdot}\{7\}_{(n)}{\cdot}\{17\}_{(n-1)}$, ($\{17\}_{(n-1)}$ from row above).
Column {13}: From Eq. (A.8). $E = 0.01{\cdot}\Delta t_{(n)}{\cdot}\bar{t}_{(n)}{\cdot}(\Sigma(\Delta A_p/\bar{r}_p))_{(n-1)} = 0.01{\cdot}\{7\}_{(n)}{\cdot}\{8\}_{(n)}{\cdot}\{19\}_{(n-1)}$, ($\{19\}_{(n-1)}$ from row above).
Column {14}: From Eq. (A.5). $\Delta V_p = (\Delta V - D + E){\cdot}Q = (\{11\} - \{12\} + \{13\}){\cdot}\{9\}$.
Column {15}: $(\Sigma\Delta V_p)_{(n)} = \Delta V_{p(n)} + (\Sigma\Delta V_p)_{(n-1)} = \{14\}_{(n)} + \{15\}_{(n-1)}$, ($\{15\}_{(n-1)}$ from row above). The first value of the column (at 0.955 of p/p^0) is zero.
Column {16}: From Eq. (A.9). $\Delta A_p = 2{\cdot}\Delta V_p/\bar{r}_p = 2{\cdot}\{14\}/\{5\}$.
Column {17}: $(\Sigma\Delta A_p)_{(n)} = \Delta A_{p(n)} + (\Sigma\Delta A_p)_{(n-1)} = \{16\}_{(n)} + \{17\}_{(n-1)}$, ($\{17\}_{(n-1)}$ from row above). The first value of the column (at 0.955 of p/p^0) is zero.
Column {18}: $\Delta A_p/\bar{r}_p = \{16\}/\{5\}$.
Column {19}: $(\Sigma(\Delta A_p/\bar{r}_p))_{(n)} = (\Delta A_p/\bar{r}_p)_{(n)} + (\Sigma(\Delta A_p/\bar{r}_p))_{(n-1)} = \{18\}_{(n)} + \{19\}_{(n-1)}$, ($\{19\}_{(n-1)}$ from row above). The first value of the column (at 0.955 of p/p^0) is zero.
Column {20}: From Eq. (A.10). $L_p = (\Delta A_p/\bar{r}_p)/(2{\cdot}\pi) = \{18\}/(2{\cdot}\pi)$.
Column {21}: $dV_p/dw_p = 2{\cdot}\{14\}/\{4\}$.

$$R = \left(\frac{\bar{r}_{p_n}}{\bar{r}_{p_n} - t_n}\right)^3 \tag{A.12}$$

$$F = \Delta t_n \cdot \sum_{i=1}^{n-1} \frac{3 \cdot \Delta V_{p_i}}{\bar{r}_{p_i}} = \Delta t_n \cdot \sum_{i=1}^{n-1} \Delta A_{p_i} \tag{A.13}$$

$$G = \Delta t_n \cdot \bar{t}_n \cdot \sum_{i=1}^{n-1} \frac{6 \cdot \Delta V_{p_i}}{(\bar{r}_{p_i})^2} = 2 \cdot \Delta t_n \cdot \bar{t}_n \cdot \sum_{i=1}^{n-1} \frac{\Delta A_{p_i}}{\bar{r}_{p_i}} \tag{A.14}$$

$$H = \Delta t_n \cdot (\bar{t}_n)^2 \cdot \sum_{i=1}^{n-1} \frac{3 \cdot \Delta V_{p_i}}{(\bar{r}_{p_i})^3} = \Delta t_n \cdot (\bar{t}_n)^2 \cdot \sum_{i=1}^{n-1} \frac{\Delta A_{p_i}}{(\bar{r}_{p_i})^2} \tag{A.15}$$

where ΔA_{p_n} corresponds to the pore area (based on the geometry of the sphere) for the pore radius ($\bar{r}_{p_n}$), determined by Eq. (A.16).

$$\Delta A_{p_n} = \frac{3 \cdot \Delta V_{p_n}}{\bar{r}_{p_n}} \tag{A.16}$$

Describing the Eq. (A.11), the term $(F - G + H)$ refers to the change of multilayer adsorbed volume of spherical pores larger than $\bar{r}_{p_n}$, thus the term $\Delta V_n - (F - G + H)$ is the change of the volume by capillary condensation inside the $\bar{r}_{p_n}$. Therefore, this last term is corrected by multiplying by R, in order to consider the multilayer adsorption in $\bar{r}_{p_n}$ obtaining its pore volume ΔV_{p_n}.

Finally, the quantity of spherical pores ($N(\bar{r}_{p_n})$) with $\bar{r}_{p_n}$ radius was obtained with Eq. (A.17).

$$N(\bar{r}_{p_n}) = \frac{\Delta V_{p_n}}{\frac{4}{3} \cdot \pi \cdot (\bar{r}_{p_n})^3} = \left(\frac{1}{4 \cdot \pi}\right) \cdot \left(\frac{\Delta A_{p_n}}{(\bar{r}_{p_n})^2}\right) \tag{A.17}$$

Once the whole range of p/p^0 is covered, the *data base* ($\bar{r}_{p_n}$, $N(\bar{r}_{p_n})$) is obtained. From this data base, the simulated adsorption isotherm for a given value of f_c is plotted. As an example, the Table A.2 illustrates the detailed mathematical steps to obtain this data base using the completed adsorption branch data of the experimental nitrogen isotherm of the SBA-16 sample using a f_c value of 0.5 nm.

In Table A.2, columns {1} and {8} are the completed nitrogen isotherm data (range between 0.050 and 0.955 of p/p^0 at intervals of 0.005). Columns {2} to {20} are calculated for the application of Eq. (A.11) using the BJH algorithm. From the last mentioned values, the data base for spherical pores ($\bar{r}_{p_n}$, $N(\bar{r}_{p_n})$) are obtained, which values are shown in columns {3} and {21}, respectively.

A.2. Simulated isotherms

The simulated adsorption or desorption isotherms for OMM were obtained taking into account the following considerations:

Cylindrical pore

The phenomena of capillary condensation (adsorption branch) or capillary evaporation (desorption branch) are modeled assuming the formation of cylindrical (Eq. (A.1)) or hemispherical (Eq. (A.2)) meniscus, respectively.

Spherical pore

The phenomenon of capillary condensation (adsorption branch) is modeled assuming the formation of hemispherical (Eq. (A.2)) meniscus.

The simulated isotherms were constructed using the data base ($\bar{r}_{p_n}$, L_{p_n}) for cylindrical pores (Table A.1, columns {5} and {20}). Regards to spherical pores, the data base ($\bar{r}_{p_n}$, $N(\bar{r}_{p_n})$) was used (Table A.2, columns {3} and {21}).

The simulated adsorption or desorption isotherms, are constructed by using the relative pressure data of the completed isotherm (starting from 0.050). For each p/p^0 value, from the corresponding modified Kelvin radius (Eq. (A.1) or (A.2)) and the t value (Eq. (A.4)), a ***pore radius value*** (Eq. (A.3)) is calculated. If the data base ($\bar{r}_{p_n}$, L_{p_n}) or ($\bar{r}_{p_n}$, $N(\bar{r}_{p_n})$), as appropriate, contains pores with sizes *equal to or smaller* than this ***pore radius value***, then these pores will completely condensate/evaporate, filling/emptying their volumes (ΔV_p). In contrast, the pores (from data base) with sizes *higher* than this ***pore radius value***, will only contribute to the adsorbed/desorbed volume with the adsorbed layer on their walls, which depends of the pore geometry (cylindrical Eq. (A.18) and spherical pore Eq. (A.19)).

$$\pi \cdot \left[(\bar{r}_p)^2 - (\bar{r}_p - t)^2\right] \cdot L_p \tag{A.18}$$

$$\frac{4}{3} \cdot \pi \cdot \left[(\bar{r}_p)^3 - (\bar{r}_p - t)^3\right] \cdot N(\bar{r}_p) \tag{A.19}$$

Therefore, for a given p/p^0 value, the adsorbed volume in the mesopores (V_{meso}) corresponds to the sum of all the adsorbed volume contributions of each pore present in the data base.

If the OMM has micropores, this volume (obtained by α_s-plot method following the criteria above described) should be added to the total adsorbed volume ($V_{ads} = V_{meso} + V_{\mu p}$).

Repeating the same procedure for each value of p/p^0 up to the last value (0.955), the simulated adsorption or desorption isotherm (p/p^0 vs V_{ads}) is obtained.

In order to exemplify the construction of a desorption simulated isotherm from the data base obtained in Table A.1 (in this case SBA-15_S3 sample and $f_c = 0.3$ nm), the detailed mathematical steps for *cylindrical pores* are shown in Table A.3, in which rows [a] and [b] represent the data base ($\bar{r}_{p_n}$, L_{p_n}) taken from columns {5} and {20} of the Table A.1. Row [c] are the pore volumes corresponding (ΔV_p) to these data base (Table A.1, column {14}). Column {5} corresponds to the total adsorbed volume (V_{ads}) given by the sum of adsorbed volume in the mesopores (V_{meso}, column {4}) and the micropore volume ($V_{\mu p}$) of the sample. Columns {6} to {k} are the adsorbed volume contribution of each pore of the data base ($\bar{r}_{p_n}$, L_{p_n}). For instance, taking a $\bar{r}_p$ (row [a]) equal to ***3.63 nm*** (see shadowed columns in Table A.3), at p/p^0 of 0.050 the corresponding pore radius value is 1.076 nm (column {3}). This last value is smaller than the first one; therefore, for this pore size the contribution to the adsorbed volume (for this p/p^0 value) is only given by the adsorbed layer on their walls (Eq. (A.18)). This contribution is given until p/p^0 values of 0.665 where the corresponding pore radius value is 3.61 nm. For the next p/p^0 value (0.670) the corresponding pore radius value is 3.66 nm, which is higher than $\bar{r}_p$, then, from here a total evaporation (or condensation if the adsorption branch was chosen) inside the pore $\bar{r}_p$ occurs and the contribution to the adsorbed volume is given by its pore volume ΔV_p (118.4 $mm^3\ g^{-1}$).

As it can be seen, Table A.3 is divided by a stepwise line, where in the bottom the total evaporation inside the pores has already been occurred.

The same procedure is used to construct the simulated adsorption isotherms for *spherical* pores. In this case, in the Table A.3 the rows [a] and [b] are the data base ($\bar{r}_{p_n}$, $N(\bar{r}_{p_n})$) taken from columns {3} and {21} of the Table A.2. Row [c] are the pore volumes corresponding (ΔV_p) to these data base (Table A.2, column {13}). Columns {6} to {k} are the adsorbed volume contribution of each pore of the data base ($\bar{r}_{p_n}$, $N(\bar{r}_{p_n})$), where Eq. (A.19) is used instead of Eq. (A.18).

Thus, if several f_c values are selected, a series of simulated isotherms is obtained. Then, it is possible to find a *final correction term, which* simulated isotherm adjusts to the experimental one.

Table A.2
Calculation of the data base ($\bar{r}_{p_n}$,$N(\bar{r}_{p_n})$) for OMM with *spherical pores*, using a value of correction term (f_c) of 0.5 nm.

	{1}	{2}	{3}	{4}	{5}	{6}	{7}	{8}	{9}	{10}	{11}	{12}	{13}	{14}	{15}	{16}	{17}	{18}	{19}	{20}	{21}	{22}
	p/p^0	Δr_p	$\bar{r}_p$	t	Δt	$\bar{t}$	R	V	ΔV	F	G	H	ΔV_p	$\Sigma\Delta V_p$	ΔA_p	$\Sigma\Delta A_p$	$\Delta A_p/\bar{r}_p$	$\Sigma(\Delta A_p/\bar{r}_p)$	$\Delta A_p/(\bar{r}_p)^2$	$\Sigma(\Delta A_p/(\bar{r}_p)^2)$	$N(\bar{r}_p)$	dV_p/dw_p
				(nm)				($mm^3\ g^{-1}$)							($m^2\ g^{-1}$)		($m^2\ g^{-1}\ nm^{-1}$)		($m^2\ g^{-1}\ nm^{-2}$)			($mm^3\ g^{-1}\ nm^{-1}$)
0	0.955			1.66				627.0						0		0		0		0		
1	0.950	2.17	21.98	1.64	0.029	1.65	1.26	626.6	0.37	0	0	0	0.47	0.47	0.06	0.06	0.003	0.003	$1{\cdot}10^{-4}$	$1{\cdot}10^{-4}$	$1.05{\cdot}10^{-5}$	0.43
2	0.945	1.78	20.00	1.61	0.027	1.62	1.29	626.3	0.36	0.002	$3{\cdot}10^{-4}$	$9{\cdot}10^{-6}$	0.46	0.92	0.07	0.13	0.003	0.006	$2{\cdot}10^{-4}$	$3{\cdot}10^{-4}$	$1.36{\cdot}10^{-5}$	0.51
3	0.940	1.48	18.37	1.58	0.026	1.60	1.31	625.9	0.37	0.003	$5{\cdot}10^{-4}$	$2{\cdot}10^{-5}$	0.48	1.41	0.08	0.21	0.004	0.010	$2{\cdot}10^{-4}$	$5{\cdot}10^{-4}$	$1.86{\cdot}10^{-5}$	0.65
4	0.935	1.26	17.00	1.56	0.025	1.57	1.33	625.6	0.36	0.005	$8{\cdot}10^{-4}$	$3{\cdot}10^{-5}$	0.47	1.88	0.08	0.29	0.005	0.015	$3{\cdot}10^{-4}$	$8{\cdot}10^{-4}$	$2.28{\cdot}10^{-5}$	0.75
.	...	...	...	...	...	...	...	...	...	...	...	...	...	...	...	...	...	...	...	...	...	...
.	0.670	0.052	3.88	0.957	0.006	0.960	2.34	573.5	10.0	0.359	0.162	0.019	22.9	111.5	17.7	76.9	4.5	18.5	1.2	4.5	0.0931	888
.	0.665	0.050	3.83	0.951	0.006	0.954	2.35	561.6	11.9	0.459	0.211	0.025	27.3	138.8	21.4	98.3	5.6	24.1	1.5	6.0	0.116	1090
.	0.660	0.049	3.78	0.945	0.006	0.948	2.37	548.4	13.2	0.579	0.269	0.032	30.5	169.3	24.1	122.5	6.4	30.5	1.7	7.7	0.134	1250
.	0.655	0.047	3.74	0.939	0.006	0.942	2.38	535.9	12.5	0.711	0.333	0.040	28.9	198.2	23.2	145.7	6.2	36.7	1.7	9.3	0.132	1220
.	0.650	0.046	3.69	0.933	0.006	0.936	2.40	524.7	11.2	0.833	0.393	0.047	25.6	223.8	20.8	166.5	5.6	42.3	1.5	11	0.122	1110
.	0.645	0.045	3.64	0.928	0.006	0.931	2.41	515.0	9.7	0.940	0.444	0.053	22.1	245.9	18.2	184.7	5.0	47.3	1.4	12	0.109	983
.	...	...	...	...	...	...	...	...	...	...	...	...	...	...	...	...	...	...	...	...	...	...
.	0.065	0.015	1.331	0.471	0.005	0.474	3.71	279.6	3.7	3.416	1.434	0.175	5.61	609.8	12.6	690.6	9.5	310	7.1	162	0.568	756
$n-2$	0.060	0.015	1.316	0.466	0.005	0.469	3.72	275.7	3.9	3.616	1.522	0.186	6.18	615.9	14.1	704.7	10.7	321	8.1	170	0.648	811
$n-1$	0.055	0.016	1.300	0.461	0.005	0.464	3.72	271.4	4.3	3.853	1.625	0.199	7.02	623.0	16.2	720.9	12.4	333	9.6	179	0.762	892
n	0.050	0.016	1.284	0.455	0.006	0.458	3.71	266.6	4.7	4.136	1.750	0.216	7.97	630.9	18.6	739.5	14.5	348	11.3	191	0.899	979

Column {1}: p/p^0 values from 0.955 to 0.050 (with intervals of 0.005).
Columns {2} and {3}: Both calculated (using the same procedure described for columns {4} and {5} of Table A.1) from the pore radius (r_p) obtained by Eq. (A.3) ($r_p = r_K + t$), using the modified Kelvin radius (r_K) for a hemispherical meniscus (Eq. (A.2)) and the t value (Eq. (A.4)). In this example the selected f_c value is 0.5 nm.
Column {4}: Calculated from Eq. (A.4).
Column {5}: $\Delta t = t_{(n-1)} - t_{(n)} = \{4\}_{(n-1)} - \{4\}_{(n)}$, ($\{4\}_{(n-1)}$ from row above).
Column {6}: $\bar{t} = 0.5{\cdot}(t_{(n-1)} + t_{(n)}) = 0.5{\cdot}(\{4\}_{(n-1)} + \{4\}_{(n)})$, ($\{4\}_{(n-1)}$ from row above).
Column {7}: From Eq. (A.12). $R = [\bar{r}_p/(\bar{r}_p - t)]^3 = [\{3\}/(\{3\} - \{4\})]^3$.
Column {8}: Amount adsorbed (as liquid) from the adsorption branch of the isotherm. V ($mm^3\ g^{-1}$) = V_{STP} ($cm^3\ g^{-1}$)·1.5468. STP: Standard Temperature and Pressure. In this example the taken values (interpolated from experimental adsorption isotherm data) are of the SBA-16 sample.
Column {9}: $\Delta V = V_{(n-1)} - V_{(n)} = \{8\}_{(n-1)} - \{8\}_{(n)}$, ($\{8\}_{(n-1)}$ from row above).
Column {10}: From Eq. (A.13). $F = \Delta t_{(n)}{\cdot}(\Sigma\Delta A_p)_{(n-1)} = \{5\}_{(n)}{\cdot}\{16\}_{(n-1)}$, ($\{16\}_{(n-1)}$ from row above).
Column {11}: From Eq. (A.14). $G = 2{\cdot}\Delta t_{(n)}{\cdot}\bar{t}_{(n)}{\cdot}(\Sigma(\Delta A_p/\bar{r}_p))_{(n-1)} = 2{\cdot}\{5\}_{(n)}{\cdot}\{6\}_{(n)}{\cdot}\{18\}_{(n-1)}$, ($\{18\}_{(n-1)}$ from row above).
Column {12}: From Eq. (A.15). $H = \Delta t_{(n)}{\cdot}(\bar{t}_{(n)})^2{\cdot}(\Sigma(\Delta A_p/(\bar{r}_p)^2))_{(n-1)} = \{5\}_{(n)}{\cdot}(\{6\}_{(n)})^2{\cdot}\{20\}_{(n-1)}$, ($\{20\}_{(n-1)}$ from row above).
Column {13}: From Eq. (A.11). $\Delta V_p = (\Delta V - F + G - H){\cdot}R = (\{9\} - \{10\} + \{11\} - \{12\}){\cdot}\{7\}$.
Column {14}: $(\Sigma\Delta V_p)_{(n)} = \Delta V_{p(n)} + (\Sigma\Delta V_p)_{(n-1)} = \{13\}_{(n)} + \{14\}_{(n-1)}$, ($\{14\}_{(n-1)}$ from row above). The first value of the column (at 0.955 of p/p^0) is zero.
Column {15}: From Eq. (A.16). $\Delta A_p = 3{\cdot}\Delta V_p/\bar{r}_p = 3{\cdot}\{13\}/\{3\}$.
Column {16}: $(\Sigma\Delta A_p)_{(n)} = \Delta A_{p(n)} + (\Sigma\Delta A_p)_{(n-1)} = \{15\}_{(n)} + \{16\}_{(n-1)}$, ($\{16\}_{(n-1)}$ from row above). The first value of the column (at 0.955 of p/p^0) is zero.
Column {17}: $\Delta A_p/\bar{r}_p = \{15\}/\{3\}$.
Column {18}: $(\Sigma(\Delta A_p/\bar{r}_p))_{(n)} = (\Delta A_p/\bar{r}_p)_{(n)} + (\Sigma(\Delta A_p/\bar{r}_p))_{(n-1)} = \{17\}_{(n)} + \{18\}_{(n-1)}$, ($\{18\}_{(n-1)}$ from row above). The first value of the column (at 0.955 of p/p^0) is zero.
Column {19}: $\Delta A_p/(\bar{r}_p)^2 = \{15\}/\{3\}^2$.
Column {20}: $(\Sigma(\Delta A_p/(\bar{r}_p)^2))_{(n)} = (\Delta A_p/(\bar{r}_p)^2)_{(n)} + (\Sigma(\Delta A_p/(\bar{r}_p)^2))_{(n-1)} = \{19\}_{(n)} + \{20\}_{(n-1)}$, ($\{20\}_{(n-1)}$ from row above).
Column {21}: From Eq. (A.17). $N(\bar{r}_p) = (\Delta A_p/(\bar{r}_p)^2)/(4{\cdot}\pi) = \{19\}/(4{\cdot}\pi)$.
Column {22}: $dV_p/dw_p = 2{\cdot}\{13\}/\{2\}$.

Table A.3
Calculation of the simulated isotherm for the example of the Table A.1 (*cylindrical pore*).

			[a] → $\bar{r}_p$ (nm)	1.084	1.100	1.116	1.131	…	3.54	3.58	***3.63***	3.68	3.74	3.79	…	16.80	18.17	19.80	21.78
			[b] → L_p ($m^2\,g^{-1}\,nm^{-1}$)	1.59	1.37	1.19	1.07	…	1.83	2.47	2.85	2.90	2.43	1.47	…	0.0027	0.0025	0.0024	0.0023
			[c] → ΔV_p ($mm^3\,g^{-1}$)	5.88	5.22	4.66	4.30	…	72.0	99.6	***118.4***	123.6	106.8	66.1	…	2.36	2.62	2.92	3.42
	{1}	{2}	{3}	{4}	{5}	{6}	{7}	{8}	{9}	{…}	{…}	{…}	{…}	{…}	{…}	{…}	{…}	{…}	{k-2}	{k-1}	{k}
	p/p^0	t (nm)	r_p (nm)	V_{meso} ($mm^3\,g^{-1}$)	V_{ads} ($mm^3\,g^{-1}$)	*Adsorbed volume contribution of each pore* ($mm^3\,g^{-1}$)															
1	0.050	0.455	1.076	306.9	356.6	3.90	3.43	3.02	2.76	…	17.3	23.7	27.8	28.6	24.4	14.9	…	0.13	0.13	0.13	0.14
2	0.055	0.461	1.092	312.3	362.0	5.88	3.46	3.05	2.79	…	17.5	23.9	28.1	29.0	24.7	15.1	…	0.13	0.13	0.13	0.14
3	0.060	0.466	1.108	317.3	367.0	5.88	5.22	3.08	2.81	…	17.7	24.2	28.4	29.3	25.0	15.3	…	0.13	0.13	0.14	0.14
4	0.065	0.471	1.123	321.9	371.6	5.88	5.22	4.66	2.83	…	17.9	24.5	28.7	29.6	25.2	15.4	…	0.13	0.13	0.14	0.15
5	0.070	0.477	1.138	326.2	376.0	5.88	5.22	4.66	4.30	…	18.1	24.7	29.0	29.9	25.5	15.6	…	0.13	0.14	0.14	0.15
.	…	…	…	…	…	…	…	…	…	…	…	…	…	…	…	…	…	…	…	…	…
.	0.660	0.945	3.56	712.3	762.1	5.88	5.22	4.66	4.30	…	72.0	45.6	53.6	55.3	47.2	28.9	…	0.26	0.27	0.27	0.29
.	0.665	0.951	3.61	767.6	817.4	5.88	5.22	4.66	4.30	…	72.0	99.6	53.9	55.6	47.4	29.0	…	0.26	0.27	0.27	0.29
.	0.670	0.957	***3.66***	833.2	883.0	5.88	5.22	4.66	4.30	…	72.0	99.6	***118.4***	55.9	47.7	29.2	…	0.26	0.27	0.28	0.29
.	0.675	0.963	3.71	901.8	951.5	5.88	5.22	4.66	4.30	…	72.0	99.6	118.4	123.6	47.9	29.3	…	0.26	0.27	0.28	0.30
.	0.680	0.969	3.76	961.1	1010.9	5.88	5.22	4.66	4.30	…	72.0	99.6	118.4	123.6	106.8	29.5	…	0.26	0.27	0.28	0.30
.	0.685	0.975	3.82	998.1	1047.9	5.88	5.22	4.66	4.30	…	72.0	99.6	118.4	123.6	106.8	66.1	…	0.27	0.27	0.28	0.30
.	…	…	…	…	…	…	…	…	…	…	…	…	…	…	…	…	…	…	…	…	…
.	0.935	1.56	16.17	1108.6	1158.4	5.88	5.22	4.66	4.30	…	72.0	99.6	118.4	123.6	106.8	66.1	…	0.42	0.43	0.44	0.47
.	0.940	1.58	17.43	1110.6	1160.4	5.88	5.22	4.66	4.30	…	72.0	99.6	118.4	123.6	106.8	66.1	…	2.36	0.44	0.45	0.48
n-2	0.945	1.61	18.91	1112.8	1162.5	5.88	5.22	4.66	4.30	…	72.0	99.6	118.4	123.6	106.8	66.1	…	2.36	2.62	0.46	0.49
n-1	0.950	1.64	20.69	1115.3	1165.0	5.88	5.22	4.66	4.30	…	72.0	99.6	118.4	123.6	106.8	66.1	…	2.36	2.62	2.92	0.49
n	0.955	1.66	22.86	1118.2	1167.9	5.88	5.22	4.66	4.30	…	72.0	99.6	118.4	123.6	106.8	66.1	…	2.36	2.62	2.92	3.42

Rows [a] and [b]: Data base ($\bar{r}_{p_n}$, L_{p_n}) taken from columns {5} and {20} of the Table A.1, respectively.

Row [c]: Pore volume of the pore radius ($\bar{r}_{p_n}$) taken from column {14} of the Table A.1.

Column {1}: p/p^0 values between 0.050 and 0.955 taken with increases of 0.005 of p/p^0.
Column {2}: t values, calculated from Eq. (A.4).
Column {3}: r_p values, calculated from Eq. (A.3) using the modified Kelvin radius, cylindrical or hemispherical meniscus, as appropriate.
Column {4}: Adsorbed volume in the mesopores (V_{meso}) for a given p/p^0 value. This volume is the sum of all adsorbed volume contributions of each pore size.
V_{meso} = {6} + {7} + ⋯ + {k}.
Column {5}: Total adsorbed volume, taking into account the amount of micropores. $V_{ads} = V_{meso} + V_{\mu p}$. In this example, for SBA-15_S3 sample, the micropore volume is 49.8 $mm^3\,g^{-1}$ (see Table 1).
Columns {6} to {k}: Adsorbed volume contribution of each pore. If the pore size corresponding to the data base (row [a]) is *higher* than the pore radius value (column {3}), for a given p/p^0 value, the contribution is given by Eq. (A.18):

$$\pi\cdot((\bar{r}_p)^2-(\bar{r}_p-t)^2)\cdot L_p = \pi\cdot([a]^2-([a]-\{2\})^2)\cdot[b].$$

In contrast, if this pore size of the data base (row [a]) is *equal to* or *smaller* than the pore radius value (column {3}) for a given p/p^0 value, the contribution is: ΔV_p = [c].

Rows [a] and [b]: Data base ($\bar{r}_{p_n}$, L_{p_n}) taken from columns {5} and {20} of the Table A.1, respectively.
Row [c]: Pore volume of the pore radius ($\bar{r}_{p_n}$) taken from column {14} of the Table A.1.
Column {1}: p/p^0 values between 0.050 and 0.955 taken with increases of 0.005 of p/p^0.
Column {2}: t values, calculated from Eq. (A.4).
Column {3}: r_p values, calculated from Eq. (A.3) using the modified Kelvin radius, cylindrical or hemispherical meniscus, as appropriate.
Column {4}: Adsorbed volume in the mesopores (V_{meso}) for a given p/p^0 value. This volume is the sum of all adsorbed volume contributions of each pore size.
V_{meso} = {6} + {7} + ⋯ + {k}.
Column {5}: Total adsorbed volume, taking into account the amount of micropores. $V_{ads} = V_{meso} + V_{\mu p}$. In this example, for SBA-15_S3 sample, the micropore volume is 49.8 $mm^3\,g^{-1}$ (see Table 1).
Columns {6} to {k}: Adsorbed volume contribution of each pore. If the pore size corresponding to the data base (row [a]) is *higher* than the pore radius value (column {3}), for a given p/p^0 value, the contribution is given by Eq. (A.18):
$\pi\cdot((\bar{r}_p)^2-(\bar{r}_p-t)^2)\cdot L_p = \pi\cdot([a]^2-([a]-\{2\})^2)\cdot[b]$.
In contrast, if this pore size of the data base (row [a]) is *equal to* or *smaller* than the pore radius value (column {3}) for a given p/p^0 value, the contribution is: ΔV_p = [c].

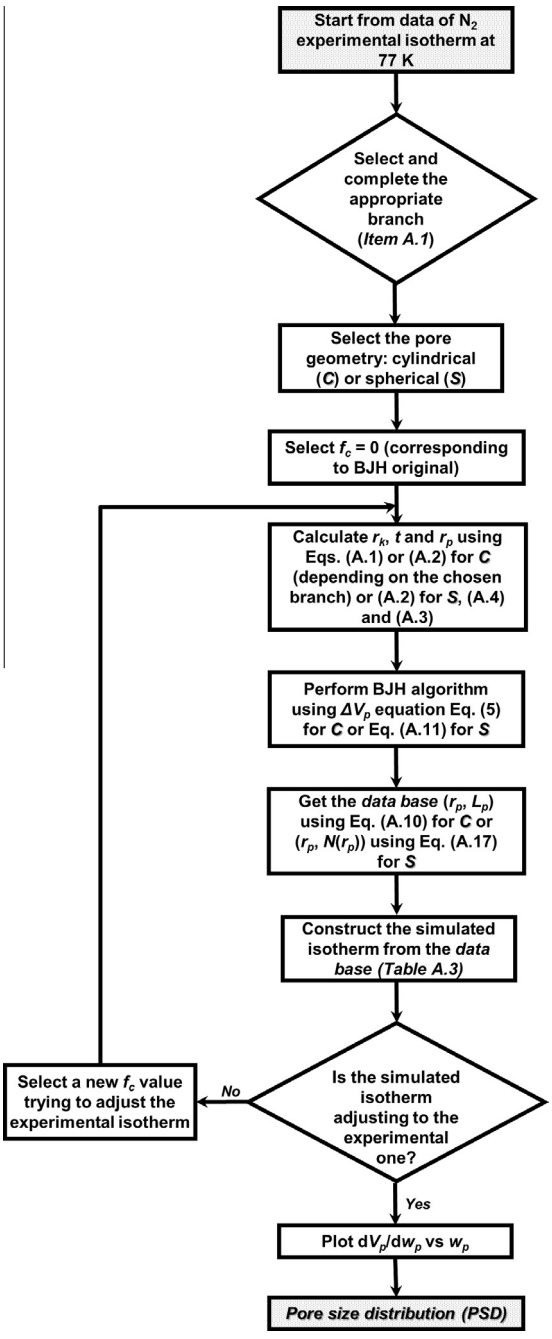

Fig. A.2. Flowchart of VBS method for OMM silica-based with cylindrical or spherical pore geometries.

A.3. Pore size distribution (PSD)

By using the final correction term value and the experimental isotherm data it is obtained the pore size distribution, which is the curve dV_p/dw_p vs. $\overline{w}_p$; where $\overline{w}_p$ is $2 \cdot \overline{r}_p$. These values are obtained from the Table A.1 (columns {21} and {5}) or A.2 (columns {22} and {3}), as appropriate, but calculated with a f_c equal to the final correction term found.

In order to schematize the application of the VBS method, Fig. A.2 shows a flowchart to apply in the type of studied samples.

References

[1] C.M. Lastoskie, K.E. Gubbins, Adv. Chem. Eng. 28 (2001) 203–250.
[2] M. Thommes, Physical adsorption characterization of ordered and amorphous mesoporous materials, in: G.Q. Lu, X.S. Zhao (Eds.), Nanoporous material, Science and Engineering, Imperial College Press, London, 2004, pp. 317–364.
[3] S.J. Gregg, K.S.W. Sing, Adsorption, Surface Area and Porosity, Academic Press, New York, 1982.
[4] F. Rouquerol, J. Rouquerol, K.S.W. Sing, P. Llewellyn, G. Maurin, Adsorption by Powders and Porous Solids: Principles, Methodology and Applications, Academic Press, San Diego, 2014.
[5] P.I. Ravikovitch, G.L. Haller, A.V. Neimark, Adv. Colloid. Interface 76–77 (1998) 203–226.
[6] C.M. Lastoskie, K.E. Gubbins, Stud. Surf. Sci. Catal. 128 (2000) 41–50.
[7] A.V. Neimark, P.I. Ravikovitch, Stud. Surf. Sci. Catal. 128 (2000) 51–60.
[8] F. Schüth, K. Sing, J. Weitkamp, Handbook of Porous Solids, Wiley, Germany, 2002.
[9] E.P. Barrett, L.G. Joyner, P.P. Halenda, J. Am. Chem. Soc. 73 (1951) 373–380.
[10] R. Montarnal, J. Phys. et Rad. 12 (1953) 732–733.
[11] D. Dollimore, G.R. Heal, J. Colloid, Interf. Sci. 33 (1970) 508–519.
[12] M. Thommes, Chem.-Ing.-Tech. 82 (2010) 1059–1073.
[13] M. Kruk, M. Jaroniec, A. Sayari, Langmuir 13 (1997) 6267–6273.
[14] X.S. Zhao, G.Q. Lu, G.J. Millar, Ind. Eng. Chem. Res. 35 (1995) 2075–2090.
[15] A. Galarneau, D. Desplantier-Giscard, F. Di Renzo, F. Fajula, Catal. Today 68 (2001) 191–200.
[16] C. Yu, B. Tian, X. Liu, J. Fan, H. Yang, Y. Zhao, Advances in mesoporous materials templated by nonionic block copolymers, in: G.Q. Lu, X.S. Zhao (Eds.), Nanoporous material, Imperial College Press, London, Science and Engineering, 2004, pp. 14–46.
[17] A.Y. Khodakov, A. Griboval-Constant, R. Bechara, V.L. Zholobenko, J. Catal. 206 (2002) 230–241.
[18] M. Iwamoto, Y. Tanaka, N. Sawamura, S. Namba, J. Am. Chem. Soc. 125 (2003) 13032–13033.
[19] T. Suzuki, M. Yamamoto, K. Fukumoto, Y. Akimoto, K. Yano, J. Catal. 251 (2007) 249–257.
[20] J. Villarroel-Rocha, D. Barrera, K. Sapag, Top. Catal. 54 (2011) 121–134.
[21] D. Barrera, J. Villarroel-Rocha, K. Sapag, Adsorpt. Sci. Technol. 29 (2011) 975–988.
[22] M. Thommes, R. Köhn, M. Fröba, Stud. Surf. Sci. Catal. 142 (2002) 1695–1702.
[23] M. Thommes, B. Smarsly, M. Groenewolt, P.I. Ravikovitch, A.V. Neimark, Langmuir 22 (2006) 756–764.
[24] C.J. Rasmussen, A. Vishnyakov, M. Thommes, B.M. Smarsly, F. Kleitz, A.V. Neimark, Langmuir 26 (2010) 10147–10157.
[25] S. Brunauer, J. Am. Chem. Soc. 60 (1938) 309–319.
[26] J. Rouquerol, P.L. Llewellyn, F. Rouquerol, Stud. Surf. Sci. Catal. 160 (2007) 49–56.
[27] M. Jaroniec, M. Kruk, J. Olivier, Langmuir 15 (1999) 5410–5413.
[28] J. Villarroel-Rocha, D. Barrera, A.A. García, Adsorpt. Sci. Technol. 31 (2013) 165–183.
[29] A. Zukal, M. Thommes, J. Cejka, Microporous Mesoporous Mater. 104 (2007) 52–58.
[30] P.I. Ravikovitch, D. Wei, W.T. Chueh, G.L. Haller, A.V. Neimark, J. Phys. Chem. B 101 (1997) 3671–3679.
[31] R.M. Grudzien, J.P. Blitz, S. Pikus, M. Jaroniec, Microporous Mesoporous Mater. 118 (2009) 68–77.
[32] S. Lowell, J.E. Shields, M.A. Thomas, M. Thommes, Characterization of Porous Solids and Powders: Surface area, Pore Size and Density, Kluwer Academic Publishers, The Netherlands, 2004.
[33] H. Naono, M. Hakuman, T. Shiono, J. Colloid, Interface Sci. 186 (1997) 360–368.
[34] P.I. Ravikovitch, A.V. Neimark, Langmuir 18 (2002) 1550–1560.
[35] W.W. Lukens, P. Schmidt-Winkel, D. Zhao, J. Feng, G.D. Stucky, Langmuir 15 (1999) 5403–5409.